JOURNAL OF GEOPHYSICAL RESEARCH, VOL. 100, NO. A12, PAGES 23,703–23,710, DECEMBER 1, 1995

ULF pulsations driven by magnetopause motions: Azimuthal phase characteristics

Andrew N. Wright and Graham J. Rickard

Department of Mathematical and Computational Sciences, University of St. Andrews
St. Andrews, Fife, Scotland

Abstract. We present numerical simulations of wave coupling in a cold, ideal, inhomogeneous plasma waveguide which approximates the flanks of the magnetosphere. Two types of driving conditions are investigated. The first corresponds to a displacement of the magnetopause over a fixed azimuthal range. The pulsations driven by this boundary condition have an azimuthal wavenumber and phase speed determined by the equilibrium structure of the magnetosphere. The second condition corresponds to a displacement pulse which runs antisunward along the magnetopause and produces pulsations with a phase velocity strictly equal to that of the boundary pulse. Our results are compared briefly with data and suggest that on some occasions the magnetosphere is driven in a fashion that is well approximated by a "running" pulse or wave on the magnetopause.

1. Introduction

Advances in observations of ULF toroidal pulsations [e.g., *Walker et al.*, 1992; *Ziesolleck and McDiarmid*, 1994] have provided a new impetus to pulsation theory. Whilst there are many details of the observations that theorists can explain, there remain a few enigmas: for example, why is there a dawn/dusk asymmetry for the pulsations? Why are *Samson et al.'s* [1992] "magic" frequencies so robust over long periods? Why do we not observe any signature of the fast mode which is thought to be responsible for driving pulsations?

In an effort to explain data, the basic resonant coupling model of *Southwood* [1974] and *Chen and Hasegawa* [1974] was refined to give the cavity model [*Kivelson and Southwood*, 1985; *Allan et al.*, 1986]. The cavity model, which explains the discrete frequencies of pulsations, has been refined recently to produce the waveguide model of the magnetosphere [e.g., *Walker et al.*, 1992; *Samson et al.*, 1992; *Harrold and Samson*, 1992; *Wright*, 1994]. The waveguide model can also explain the discrete frequencies of pulsations [*Wright*, 1994; *Rickard and Wright*, 1994]. Moreover, the fact that fast waves disperse and propagate within a waveguide may account for the absence of a coherent fast mode signature in data [*Rickard and Wright*, 1995].

The present paper extends numerical modeling of nonuniform waveguides by investigating a variety of driving conditions at the magnetopause. The correlation between driving condition and the azimuthal wavelength or azimuthal phase velocity of the pulsation is studied. We find that for a "stationary" driving pulse (one where the magnetopause is disturbed at a fixed location) the pulsations have an inherent wavelength and phase velocity that is independent of the pulse details but is determined by the equilibrium structure of the magnetosphere. When a "running" driving pulse is employed (a ripple is run along the magnetopause at constant speed) all pulsations have a phase velocity equal to the speed of the pulse. These boundary conditions may mimic the disturbance produced by a pressure pulse or density enhancement in the magnetosheath flow that is incident upon the magnetopause. For example, if a density enhancement hits the nose of the magnetopause (which is a stagnation point) it will be slow to move around the flanks and may be approximated by a "stationary" pulse. Other disturbances may impinge upon the magnetopause away from the stagnation point and be convected antisunward around the flanks (a running pulse). The latter condition may also mimic the antisunward propagation of magnetopause waves, such as Kelvin-Helmholtz disturbances [*Walker*, 1981]. Our results are compared briefly with data, and we conclude that, at least on some occasions, pulsations are likely to be excited by disturbances running antisunward along the magnetopause. The paper is structured as follows: section 2 describes the model, theoretical ideas, numerical boundary conditions, and phase calculations; the results are presented in section 3, while section 4 discusses and summarizes the main points of the paper.

2. Model

The flank of the magnetosphere is idealized by a straight waveguide as shown in Figure 1. The coordinate x spans L shells, y is equivalent to the azimuthal coordinate, and z is the field-aligned coordinate. Es-

Paper number 95JA01765.
0148-0227/95/95JA-01765$05.00

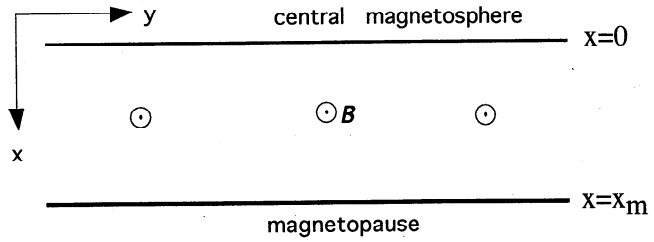

Figure 1. The waveguide and coordinate system used to describe the flanks of the magnetosphere.

sentially, we have taken the uniform field "box" model of *Southwood* [1974] and made it infinitely long. The plasma is assumed to be cold, perfectly conducting, and bounded by perfectly reflecting boundaries in both x and z. The density is independent of z, and we consider a single Fourier mode ($b_x, b_y \sim \cos(k_z z); b_z, u_x, u_y \sim \sin(k_z z)$). Thus the governing equations become [e.g., *Rickard and Wright* 1994, equation (12)]

$$\rho \frac{\partial u_x}{\partial t} = -B\left(k_z b_x + \frac{\partial b_z}{\partial x}\right) \quad (1a)$$

$$\rho \frac{\partial u_y}{\partial t} = -B\left(k_z b_y + \frac{\partial b_z}{\partial y}\right) \quad (1b)$$

$$\frac{\partial b_x}{\partial t} = k_z B u_x \quad (1c)$$

$$\frac{\partial b_y}{\partial t} = k_z B u_y \quad (1d)$$

$$\frac{\partial b_z}{\partial t} = -B\left(\frac{\partial u_x}{\partial x} + \frac{\partial u_y}{\partial y}\right) \quad (1e)$$

B is the equilibrium (uniform) field strength and ρ the equilibrium density.

In the remainder of this paper length will be normalized by x_m, velocities by the Alfvén speed at $x = 0, V(x = 0)$, density by $\rho(x = 0)$, and time by $x_m/V(x = 0)$. The Alfvén speed (V) varies with position inside the magnetosphere. For simplicity we assume that V varies only with L shell (or x) such that for $0 < x < x_c$, the normalized Alfvén speed is given by

$$V(x) = (1 - x/x_0) \quad (2)$$

For $x_c < x < 1$ we fit a parabolic density function with the boundary conditions that V and dV/dx be continuous at x_c, and $dV/dx = 0$ at $x = 1$. Thus for $x_c < x < 1$ we find

$$\frac{1}{V^2(x)} = \frac{x_0 - 2x_c + 1}{x_0(1 - x_c/x_0)^3} - \frac{(1-x)^2}{x_0(1-x_c)(1-x_c/x_0)^3} \quad (3)$$

where x_0 is an arbitrary scaling parameter that determines how rapidly V changes with L shell, and x_c is the position at which the Alfvén speed changes from the form given in (2) to that in (3)

Figure 2 shows the Alfvén speed variation when $x_c = 0.8$ and $x_0 = 0.95$, 1.0, 1.2, 1.4, 1.6, and 1.8. Evidently

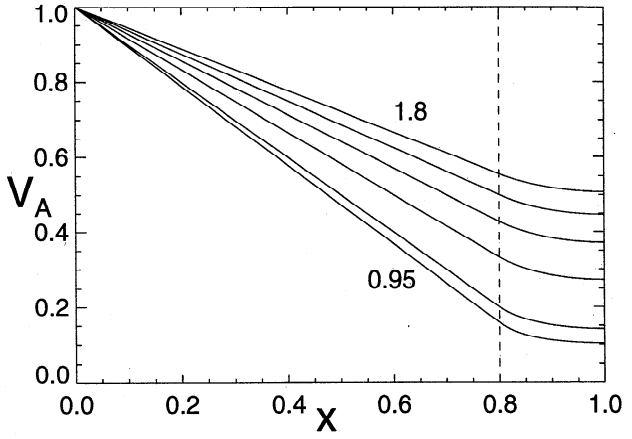

Figure 2. The variation of Alfvén speed (V_A) in the model waveguide. A variety of waveguides are employed and are parameterized by the scale length $x_0 = 0.95$, 1.0, 1.2, 1.4, 1.6, and 1.8. The vertical dashed line locates x_c.

the parameters x_0 and x_c determine the equilibrium density and Alfvén speed in our model waveguide. Later we shall use these parameters to study which properties of pulsations depend upon the equilibrium model and which are determined by the driving condition.

2.1. Theory

The waveguide theory developed by *Wright* [1994] and borne out by the simulations of *Rickard and Wright* [1994, 1995] may be summarized as follows: If a source of fast mode waves is introduced over a small region, the small k_y components will have a small group velocity along the guide and thus remain near the source region. The larger k_y components propagate relatively quickly along the guide and leave the source region. It is the small k_y components that produce a quasi-steady oscillatory fast mode driver for Alfvén resonances near the source. Consequently, pulsations with natural frequencies equal to that of the $k_y = 0$ fast mode eigenfrequencies will be excited in this region. Thus we can

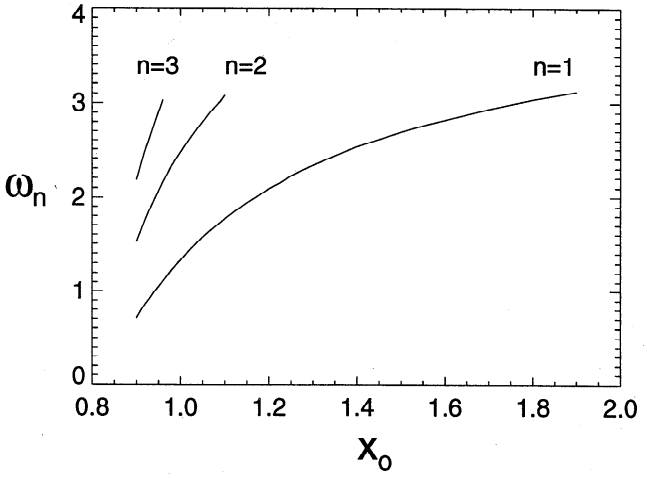

Figure 3. The ($k_y = 0$) fast eigenfrequencies of the waveguide as a function of x_0 (n is the harmonic number of the mode in x).

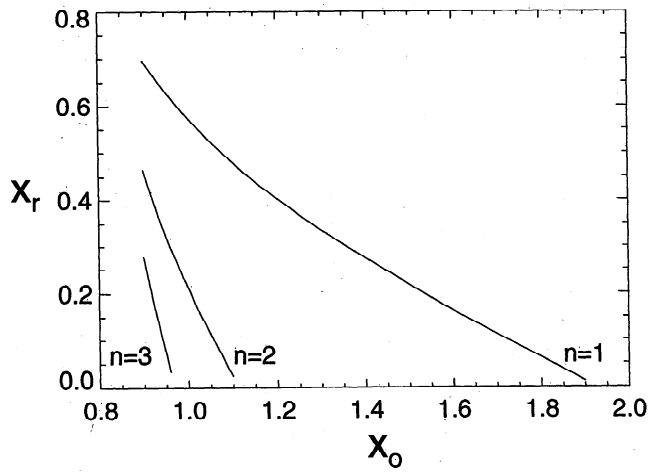

Figure 4. The expected locations of the Alfvén resonances as a function of x_0 (x_r is defined by $k_z V_A(x_r)$ equaling a fast eigenfrequency).

anticipate the frequencies of pulsations from knowledge of the equilibrium, since this determines the $k_y = 0$ fast eigenfrequencies. Throughout this paper we set $u_x = 0$ at $x = 0, 1$ (unless the boundary is being driven) and take $k_z = \pi$. Figure 3 shows how the $k_y = 0$ fast eigenfrequencies vary with the equilibrium parameter x_0 (n labels the number of the harmonic in the x direction). The Alfvén continuum spans $k_z V(x = 0)$ to $k_z V(x = 1)$, and when the fast eigenfrequencies of Figure 3 lie within the continuum we may predict the location of the pulsation (x_r) by $\omega_r = k_z V(x_r)$. The result is shown in Figure 4 for a range of x_0.

2.2. Numerical Scheme

The details of the numerical scheme have been given elsewhere [*Rickard and Wright*, 1994, 1995]. Briefly, we employ a second-order method; the leapfrog-trapezoidal algorithm. Care must be taken to resolve all time and spatial scales, particularly the phase mixing length $L_{ph} = 2\pi/(td\omega_A/dx)$, which can be a problem for large run times. The "open" boundary condition along the waveguide was achieved by adding additional sections of grid throughout each run ahead of the fast mode. ("Outgoing" boundary conditions were investigated, but all produced some unphysical wave reflection.) A symmetry boundary condition ($\partial b_z/\partial y = 0$)) was employed at $y = 0$.

2.2.1. Stationary pulse. The first type of boundary condition we employed was a "stationary pulse". This is identical to the driving employed by *Rickard and Wright* [1995]: The section of magnetopause $-\Delta y/2 < y < +\Delta y/2$ is displaced in toward the Earth and returned to its original position over a time τ.

The spatial form of the boundary displacement is

$$\xi_x = \quad 0 \quad |y| > \Delta y/2 \qquad (4a)$$

$$\xi_x = \quad (1 + \cos(2\pi y/\Delta y))/2 \quad |y| < \Delta y/2 \qquad (4b)$$

For the stationary pulse runs presented here $\tau = 3$ and $\Delta y = 0.4$, unless stated otherwise.

2.2.2. Running pulse. The second type of driving condition we investigated was a "running pulse." In this case a pulse with a spatial form similar to (4) was run along from $y \approx 0$ to $y \approx 5$ at constant speed V_b. (V_b was changed for each new run.) Thus the pulse was run along the magnetopause for $0 < t < 5/V_b$. To introduce the pulse and remove it we ramped its amplitude up over $0 < t < 0.7/V_b$ and down over $4.3/V_b < t < 5/V_b$. The product of the "ramping" function and the running spatial pulse function gave $\xi_x(y, t)$ on the magnetopause. The time derivative of ξ_x gives $u_x(x = 1, y, t)$ which is used as a boundary condition to drive the governing equations. For the "running pulse" simulations presented here $\Delta y = 1.0$, and V_b took the values 0.35, 0.7, and 1.4. (See the discussion at the end of subection 3.3 on the choice of Δy and V_b.)

At the magnetopause $\partial/\partial x$ is calculated by one-sided derivatives, while u_x is specified by the driving condition or assigned to zero following the driving phase. (See *Wright and Rickard* [1995] for a more detailed discussion.)

2.3. Phase Calculations

The phase structure of the pulsations was investigated by using the method described by *Ziesolleck and McDiarmid* [1994] who studied ground-based magnetometer data. (Note that we are calculating the fields in the magnetosphere above the ionosphere. When comparing our results with ground-based magnetometer data, the transverse fields must be turned through the Hughes rotation of 90° [*Hughes*, 1974].)

We positioned a set of stations (or "satellites", as we are measuring magnetospheric perturbations) in our simulation space and record the time history of the field perturbation. Care is taken to resolve the periods of interest. For a given station/satellite we proceed as follows: The fast Fourier transform (FFT) is taken; this produces a complex Fourier transform for each frequency bin. The phase of the signal for a given bin is found from $\tan^{-1}(I_m/R_e)$, where R_e and I_m are the real and imaginary part of the FFT for that bin. The phase is then adjusted to lie in the range $-\pi < \phi < \pi$. This process is repeated for all frequency bins. An identical procedure is repeated for the other satellites/stations. Since the phase has an ambiguity of $2n\pi$, we add/subtract such a factor to ensure that (for a given frequency bin) the phase from one satellite to the next does not change by more than π. To calculate the phase of the pulsation we normally average the phases of a few frequency bins centered upon the pulsation frequency, and then offset all these averaged phases by that averaged over all satellites, since only changes of phase are meaningful. (Note that this procedure requires the distance between consecutive satellites to be less than half of the azimuthal wavelength.)

3. Results

The numerical methods of the previous section were applied to the inhomogeneous waveguide model. We now present the results, beginning with the "stationary pulse" driving condition described in section 2.2.1.

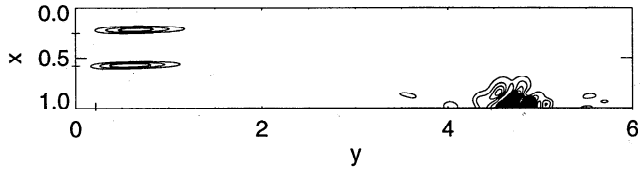

Figure 5. Contours of total energy density at $t = 40$. The waveguide has $x_0 = 1.0, k_z = \pi$ and was driven by a "stationary pulse" of extent $\Delta y = 0.4$ for a duration $\tau = 3.0$. The mark on the y axis denotes the extent of the stationary pulse, while those on the x axis indicate the anticipated x coordinates of the Alfvén resonances.

3.1. Stationary Pulse

A waveguide with $x_0 = 1.0$ was driven by the "stationary pulse" boundary condition. From Figure 4 we expect Alfvén resonances to occur at $x = 0.24$ and 0.56, where the Alfvén frequencies are 2.39 and 1.37, respectively. Figure 5 displays contours of total energy density at $t = 40$. The energy deposition in Alfvén resonances at the expected location is evident. Further down the waveguide ($y \approx 5$) the energy density is associated with fast mode waves which propagate and disperse along the guide. More details are given by *Wright* [1994] and *Rickard and Wright* [1994]. Indeed, the latter authors show how the total energy may be decomposed into Alfvénic and fast contributions (E_A and E_f, respectively),

$$E_A = \frac{1}{2}\left(\rho u_y^2 + b_y^2\right) \quad (5a)$$

$$E_f = \frac{1}{2}\left(\rho u_x^2 + b_x^2 + {b_z}^2\right) \quad (5b)$$

This partition is exact when $k_y = 0$, and a good approximation when k_y is small, such as near the Alfvén resonances. (The fast mode in Figure 5 has high k_y components, and so has significant u_y and b_y perturbations, and so would have a nonzero E_A according to (5), thus E_f is only approximately equal to the fast mode energy density.)

The time histories of E_A and E_f integrated over the entire waveguide are shown in Figure 6. Note that the total energy density ($E_A + E_f$) rises over the driving interval $0 < t < 3$ and thereafter is constant. At $t = 3$ most of the energy resides in the fast mode, but as time passes it decreases through coupling to the Alfvén mode. (The small oscillations at larger times reflect the fact that E_A and E_f are not exact representations of the fast and Alfvénic energy densities.) Figure 7 displays the azimuthal structure of the two pulsations by plotting b_y and E_A as a function of y for $x = 0.24$ and 0.564. The b_y plot shows some dominant azimuthal wavelength. At present we do not have an explanation for the dominance of any particular wavelength, nor for the nodes that occur in the E_A profile. Perhaps these are a result of the complicated interference pattern that will be produced by the low k_y fast nodes as they propagate down the guide at different group velocities. (The nonzero values of E_A over the range $4 < y < 6$ are associated with the fast mode, see Figure 5.)

Most of the fast mode energy that will drive Alfvén waves has done so by $t = 25$ (Figure 6). Thus we record the field disturbances at a set of stations/satellites at y coordinates 0.5, 0.9, 1.3, 1.7, 2.1, 2.5, 2.9, 3.3 and x coordinates 0.24 and 0.564 over the interval $25 < t < 40$. Figure 8 displays the phase variation of the pulsations for both b_x and b_y signals. Calculating the gradient $d\phi/dy$ enables us to estimate the azimuthal wavelength, $\lambda_y = 360 \cdot dy/d\phi$. For Figure 8 we find

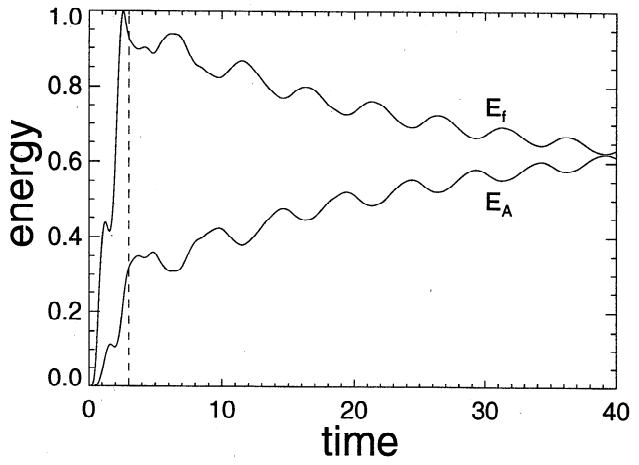

Figure 6. The time histories of the "Alfvénic" and "fast" energy densities integrated over the waveguide (same parameters as in Figure 5). The dashed line marks the end of the driving phase at $t = 3$.

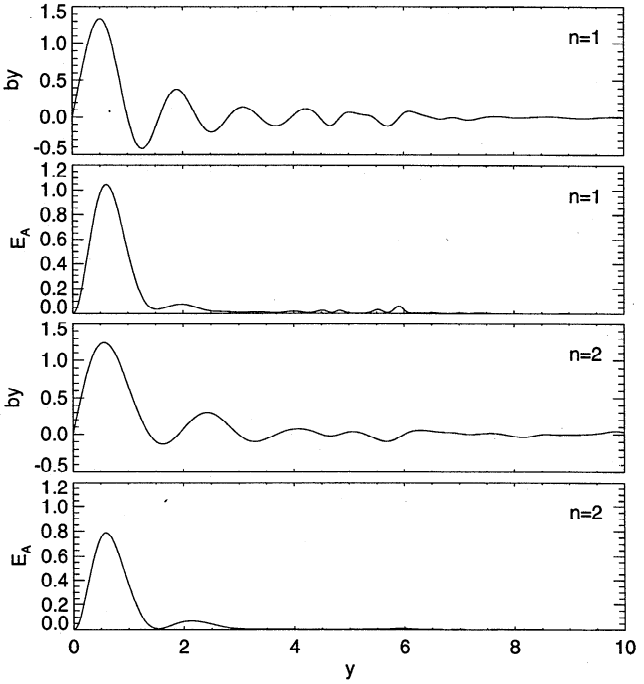

Figure 7. The variation of b_y and E_A with azimuth (y) for the first and second harmonic resonances ($x = 0.564$ and 0.24, respectively). The parameters are the same as in Figure 5.

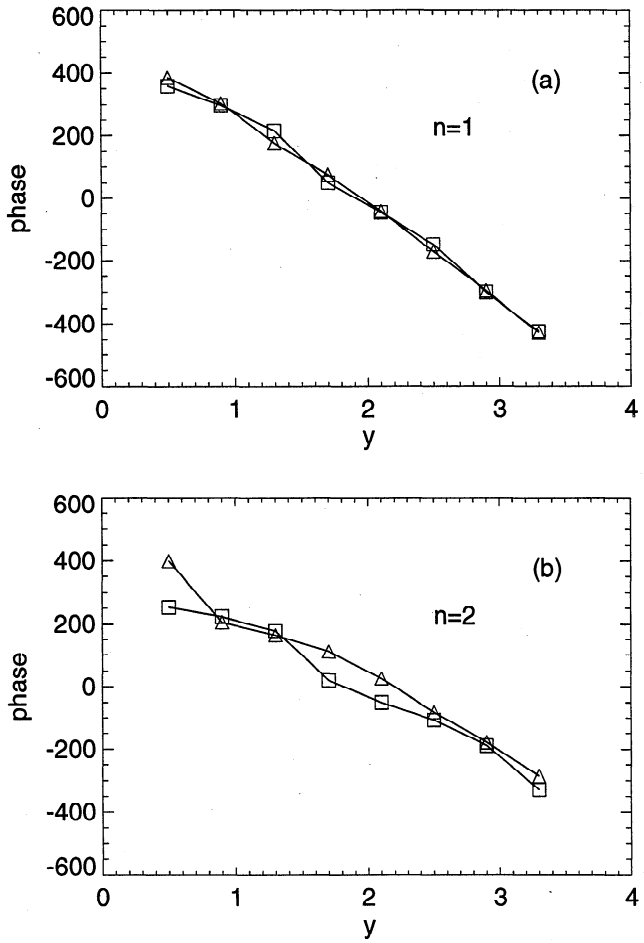

Figure 8. The phase variation of b_x (squares) and b_y (triangles), for the parameter of Figure 5, calculated over the interval $25 < t < 40$. (a) The first resonance at $x = 0.564$ used the frequency bins $0.9 < \omega < 1.45$, whilst (b) the second resonance at $x = 0.24$ employed $2.2 < \omega < 2.7$.

(after averaging the b_x and b_y gradients) $\lambda_y = 1.17$ for the $n = 1$ resonance and $\lambda_y = 1.78$ for $n = 2$. Since the resonant frequencies are $\omega_1 = 1.37$ and $\omega_2 = 2.39$, the pulsations have azimuthal phase velocities of 0.255 and 0.677, respectively ($V_p = \omega/k_y$).

We repeated identical experiments to that described above, but varied x_0 for each run. Each time we calculated the azimuthal wavelength and phase speed. The results are summarized in Figure 9. (Note that for $x_0 \geq 1.2$ our model only has one resonance.) It appears that for a stationary pulse λ_y and V_p vary systematically with x_0, that is, the equilibrium structure of the magnetosphere. It is important to decide if any other factors could be determining λ_y and V_p, for example, the width of the stationary pulse (Δy). In Figures 5 to 9, $\Delta y = 0.4$. We repeated our experiments for the model with $x_0 = 1.2$, but varied Δy from 0.12 to 1.2 and found that the structure of the pulsation was unchanged, in agreement with *Rickard and Wright* [1994]. (For $\Delta y = 0.12, 0.4$ and 1.2 λ_y was 1.60, 1.60, and 1.59, while the phase speeds were 0.532, 0.531, and 0.531, respectively.) These results suggest that the equilibrium structure of the magnetosphere determines the phase structure of pulsations driven by a stationary pulse.

3.2. Running Pulse

The next set of results employed the "running pulse" boundary condition described in section 2.2.2. We present a case study for a pulse boundary speed of $V_b = 0.7$, and $x_0 = 1.0$. Since the "running pulse" drives the waveguide for a larger time compared to the stationary pulse experiments, we run these simulations a little longer (up to $t = 50$) to allow the fast mode time to establish the resonances. Figure 10 displays similar plots to those in Figure 7. Note how E_A extends over a greater distance than previously, due to the fact that the pulse now runs over the range $0 < y < 5$. There is still a clear, coherent phase structure in the b_y signatures, and these were analyzed (along with the b_x signatures) by recording the fields over the interval $25 < t < 50$. The phase variations are displayed in Figure 11 for satellites at $x = 0.24$ and 0.564, and $y = 0.9$, 1.3, 1.7, 2.1, 2.5, 2.9, 3.3, 3.7, and 4.1. From Figure 11 we measure λ_y to be 3.32 and 1.96 for the $n = 1$ and 2 resonances, respectively. Significantly, this implies phase velocities

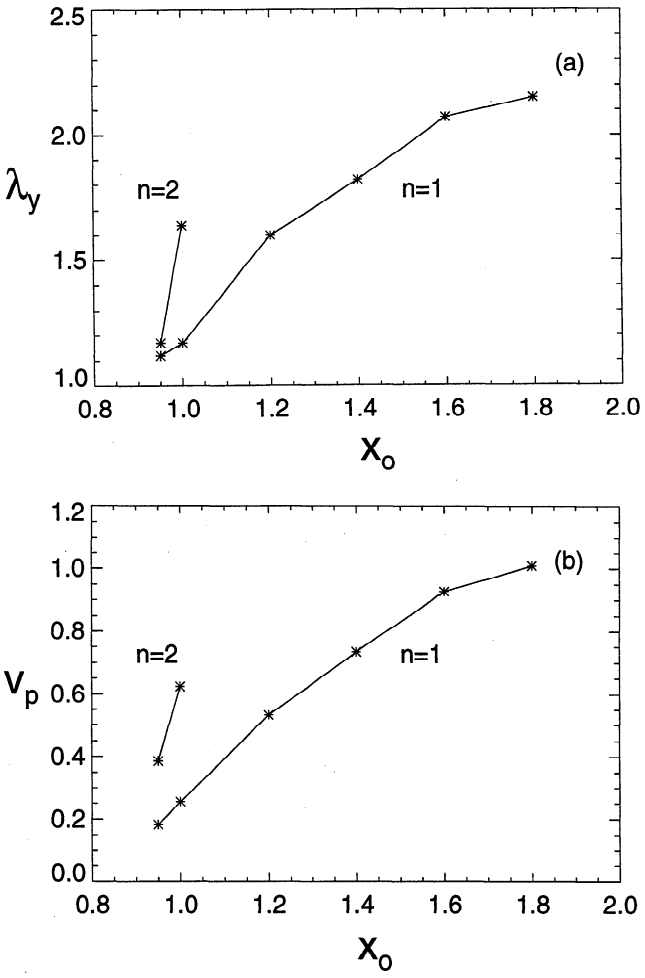

Figure 9. The variation of (a) azimuthal wavelength (λ_y) and (b) azimuthal phase speed (V_p) with x_0 when driven by a 'stationary pulse'.

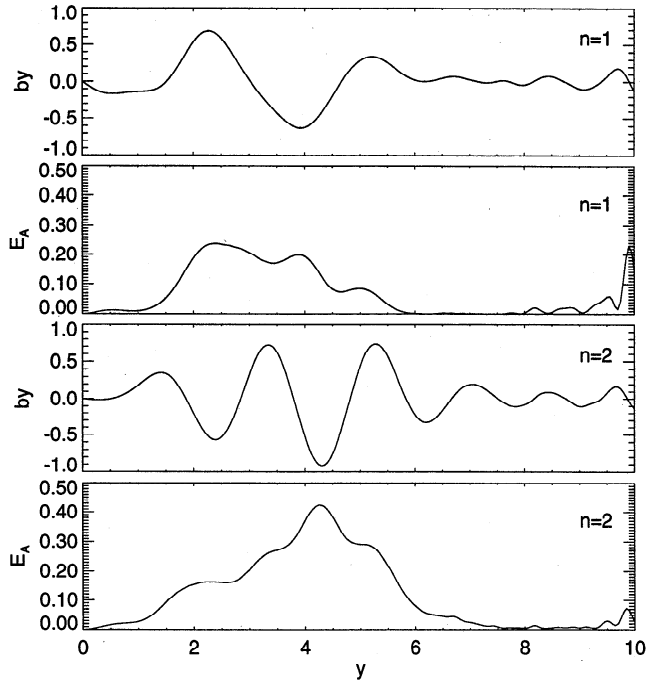

Figure 10. The same as for Figure 7, but the waveguide was excited by a running pulse ($\Delta y = 1.0, V_b = 0.7$). The snapshots were taken at $t = 50$.

of 0.72 and 0.745 for the resonances, which are essentially the same as that of the boundary pulse ($V_b = 0.7$). We note that if λ_y is estimated directly from Figure 10 by measuring the peak-to-peak distance, we find phase speeds of 0.697 and 0.698, suggesting the small discrepancy from the phase method is attributable to effects such as the finite time interval of the calculation, or the fact that the resonances may still have been growing during this interval.

The above "running pulse" experiment was repeated with two different speeds, $V_b = 0.35$ and 1.4. The azimuthal wavelengths and phase speeds were calculated, and the latter was in excellent agreement with V_b. The results are summarized in Figure 12, which plots the frequency of the Alfvén wave against the azimuthal wavenumber ($k_y = 2\pi/\lambda_y$). We have also indicated lines corresponding to phase speeds of $V_b = 0.35, 0.7$, and 1.4. The agreement between V_b and V_p of both resonances is excellent.

3.3. Coupling Efficiency

Readers may have noticed that Figure 12 does not have a point on it for the second resonance when $V_b = 0.35$, the reason being that the resonance was not driven very efficiently. To clarify this issue we display snapshots of $b_y(x)$ at $t = 50$ and $y = 3$ for the three "running pulse" experiments (Figure 13). When $V_b = 0.35$ the first Alfvén resonance (at $x = 0.564$) is excited much more strongly than the second resonance (at $x = 0.24$). For $V_b = 0.7$, the amplitude of b_y is similar for both resonances, whilst $V_b = 1.4$ favors the second resonance. Evidently, the different values of V_b excite different amounts of the low k_y waveguide modes, which in turn excite Alfvén resonances of different amplitudes.

The different coupling efficiencies may be interpreted in terms of Δy and V_b: The time it takes a point on the magnetopause to be displaced in and out is equal to $\Delta y/V_b$. Identifying this time as "half a driving period" and given $\Delta y = 1.0$, the time periods of the magnetopause displacements when $V_b = 0.35$, 0.7, and 1.4, are $\tau_m = 5.7$, 2.9, and 1.4, respectively. Thus the various boundary speeds excite waves within the magnetosphere of differing frequency spectra which will excite the two Alfvén resonances with different amplitudes. (The time periods of the two resonances are 4.59 and 2.63.) Clearly, $V_b = 0.35$ ($\tau_m = 5.7$) excites the lower-frequency resonance preferentially, whilst $V_b = 1.4$ ($\tau_m = 1.4$) favors the higher-frequency resonance. The choice of Δy and V_b were not made to represent realistic magnetospheric parameters, but for numerical convenience: A larger V_b means the pulse runs for a shorter time and reduces the computer resources required.

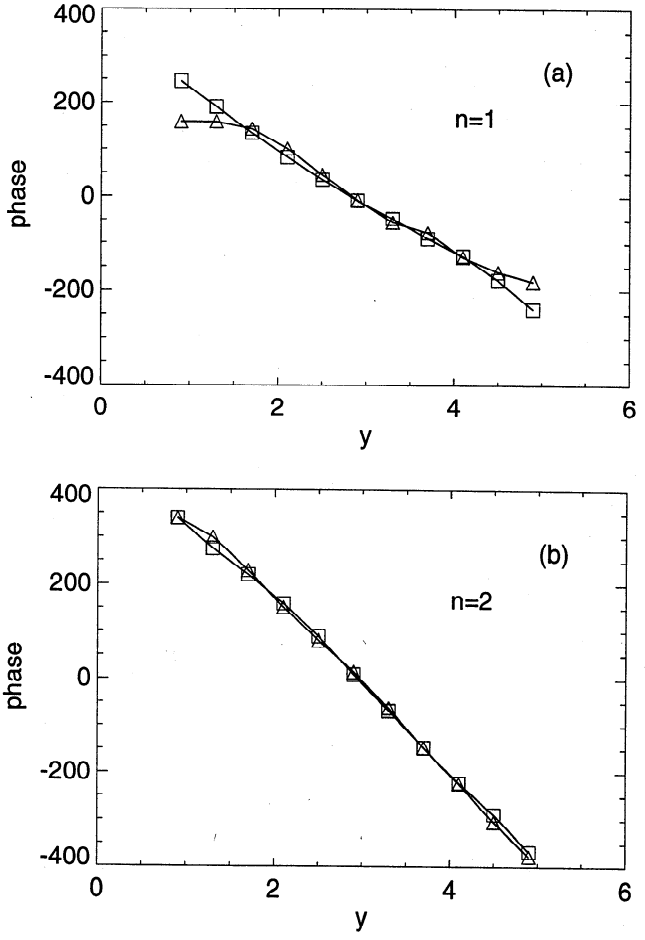

Figure 11. The phase variation of b_x (squares) and b_y (triangles) calculated on the interval $25 < t < 50$ for the "running pulse" case study (parameters as in Figure 10). (a) The first resonance at $x = 0.564$ employed the frequency band $1.13 < \omega < 1.64$. (b) The second resonance at $x = 0.24$ employed the band $2.1 < \omega < 2.7$.

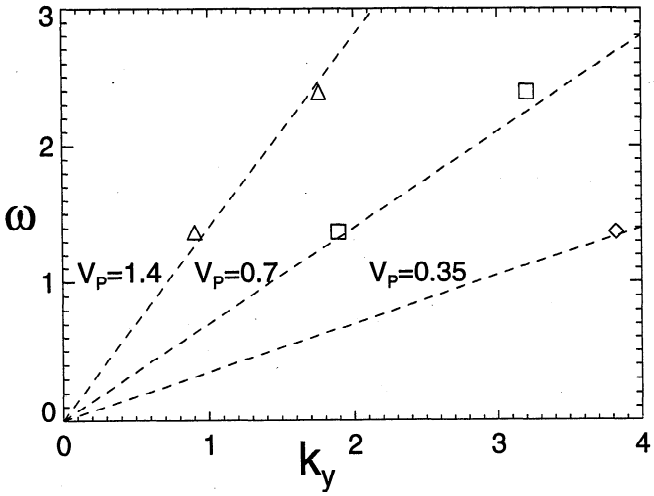

Figure 12. Pulsation frequency against azimuthal wavenumber for three 'running pulse' experiments. V_p = 0.35 (diamond), 0.7 (squares), and 1.4 (triangles). (Other parameters are as in Figure 10.)

4. Discussion and Conclusion

We have investigated the azimuthal phase structure of pulsations for two types of driving condition. The first (the "stationary pulse") reveals that each resonance has its own inherent azimuthal wavelength and phase velocity which appears to be determined by the equilibrium structure. If this type of pulsation is observed, it may be possible to infer some properties of the magnetosphere from the dependence of wavelength on equilibrium structure. Most importantly we note that if more than one resonance is driven by a "stationary pulse," their azimuthal phase velocities will be different. Thus simultaneous observations of several resonances with different phase speeds may indicate a driving source similar to our "stationary pulse."

When the "running pulse" boundary condition is used we find that the phase speed of all resonances is equal to the speed at which the pulse (or wave) moves along the boundary. Hence simultaneous observations of several resonances with equal phase speeds suggests a common source on the magnetopause. (Indeed such observations have been reported by *Ziesolleck and McDiarmid* [1994, 1995] – see Figure 16 of the former.) Our results also indicate that different magnetopause motions may excite some resonances preferentially and is potentially a useful diagnostic.

Although the results for the "stationary" and "running" pulses appear quite different, they can be understood in terms of one another; it is merely a question of what features dominate. Consider the "stationary pulse" results in Figure 7; the b_y signature of both resonances is dominated by a single hump near $y = 1$ and subsidiary ripples at larger y. The phase calculation over the range $0.5 < y < 3.3$ is essentially a calculation of the subsidiary ripples.

The running pulse boundary conditions can be synthesized from a sum of several stationary pulses: suppose at $t = 0$ we initiate a stationary pulse at $y = 0$, then at $t = 1$ we initiate a new stationary pulse at $y = 1$, and so on at $y = 2$ and $t = 2$, etc. The overall effect is that a disturbance moves along the magnetopause with a speed of $V_b = 1$. By filling in intermediate pulses at intermediate times and summing, the net effect is a smooth running pulse similar to that described in section 3.2. In the linear approximation employed here we are able to sum the boundary conditions and their associated solutions to produce more complicated solutions. Thus the "running pulse" results may be anticipated by summing a solution of the form in Figure 7 that is translated in y since the source is translated in y at later times. In this case the subsidiary ripples are not very important as we will be superposing the larger peaks from different "stationary pulse" sources. Let us concentrate upon the dominant peak. If the resonance (with period $\tau = 2\pi/\omega$) has a peak at $y \approx 1$ from a source at $y \approx 0$, then a new source at a time $\tau/2$ at $V_b\tau/2$ will produce a similar peak at $y = V_b\tau/2$. However, by this time the original peak at $y = 1$ will have oscillated to the opposite phase. Thus a phase change of π occurs over a distance $V_b\tau/2$, implying a wavelength of $\lambda_y = V_b\tau$ and a phase speed of $V_p = \omega(\lambda_y/2\pi) = V_b$.

Our results suggest that, at least on some occasions, ULF pulsations have a common source associated with antisunward propagating disturbances on the magnetopause. We do not address the origin of these disturbances, although pressure pulses or magnetopause waves may be likely candidates. Coordinated satellite and ground-based observations provide a unique opportunity for progress on this matter. Section 3.3 and Figure 13 demonstrate a relation between the speed, extent, and duration of the magnetopause displacement,

$$V_b = 2\frac{\Delta y}{\tau_m} \tag{6}$$

For a toroidal pulsation of frequency f to be excited ef-

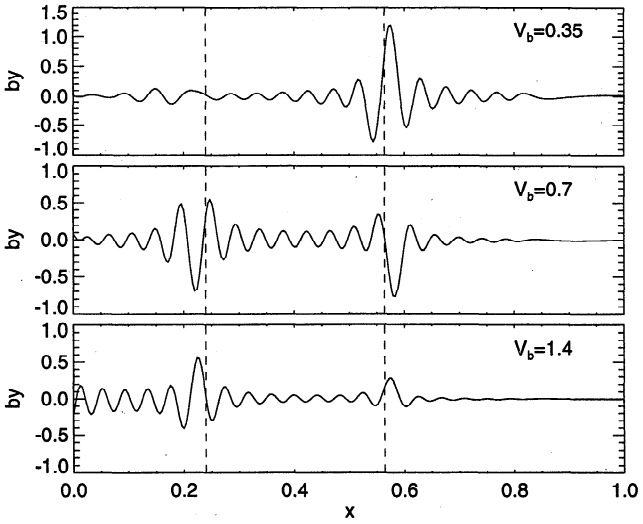

Figure 13. Snapshots of $b_y(x, y = 3)$ at $t = 50$ for the three "running pulse" experiments of Figure 12. The dashed vertical lines indicate the locations of the Alfvén resonances.

ficiently by magnetopause motions suggests that these motions occur on a timescale of $\tau_m \approx 1/f$. If satellite data can supply estimates of the azimuthal extent of the magnetopause disturbances [e.g., *Chen et al.*, 1993], then the speed of the disturbances can be calculated by (6). Comparison of the infered value of V_b with magnetosheath flow speeds and phase speeds of magnetopause surface waves and instabilities may provide a clue as to which mechanisms are important for establishing ULF toroidal pulsations. For example, *Walker* [1981] shows that the Kelvin-Helmholtz instability in a finite thickness magnetopause will have $2\Delta y \approx 20{,}000$ km, and for a typical magnetosheath flow speed of 400 km/s (V_b = 200 km/s) we find $\tau_m \approx 100$ s (Pc4 range). Thus the Kelvin-Helmholtz instability governed by a finite thickness magnetopause is probably not driver of the lower harmonic toroidal pulsations in the Pc5 range.

Acknowledgments. A. N. Wright was supported by a UK PPARC Advanced Fellowship. The authors are grateful to D. McDiarmid and C. Ziesolleck for helpful discussions concerning observations and phase analysis.

The editor thanks W. A. Bristow and A. D. M. Walker for their assistance in evaluating this paper.

References

Allan, W., S. P. White, and E. M. Poulter, Impulse-excited hydromagnetic cavity and field-line resonances in the magnetosphere, *Planet. Space Sci., 34,* 371, 1986.

Chen, L., and A. Hasegawa, A theory of long-period magnetic pulsations, 1, Steady state excitation of field line resonance, *J. Geophys. Res., 79,* 1024, 1974.

Chen, S.-H., M. G. Kivelson, J. T. Gosling, R. J. Walker, and A. J. Lazarus, Anomalous aspects of magnetosheath flow and of the shape and oscillations of the magnetopause during an interval of strongly northward interplanetary magnetic field, *J. Geophys. Res., 98,* 5727, 1993.

Harrold, B. G., and J. C. Samson, Standing ULF modes of the magnetosphere: A theory, *Geophys. Res. Lett., 19,* 1811, 1992.

Hughes, W. J., The effect of the atmosphere and ionosphere on long-period magnetospheric micropulsations, *Planet. Space Sci., 22,* 1157, 1974.

Kivelson, M. G., and D. J. Southwood, Resonant ULF waves: A new interpretation, *Geophys. Res. Lett., 12,* 49, 1985.

Rickard, G. J., and A. N. Wright, Alfvén resonance excitation and fast wave propagation in magnetospheric waveguides, *J. Geophys. Res., 99,* 13,455, 1994.

Rickard, G. J., and A. N. Wright, ULF pulsations in a magnetospheric waveguide: Comparison of real and simulated satellite data, *J. Geophys. Res., 100,* 3531, 1995.

Samson, J. C., B. G. Harrold, J. M. Ruohoniemi, and A. D. M. Walker, Field line resonances associated with MHD waveguides in the magnetosphere, *Geophys. Res. Lett., 19,* 441, 1992.

Southwood, D. J., Some features of field line resonances in the magnetosphere, *Planet. Space Sci., 22,* 483, 1974.

Walker, A. D. M., The Kelvin-Helmholtz instability in the low-latitude boundary layer, *Planet. Space Sci., 29,* 1119, 1981.

Walker, A. D. M., J. M. Ruohoniemi, K. B. Baker, R. A. Greenwald, and J. C. Samson, Spatial and temporal behaviour of ULF pulsations observed by the Goose Bay HF radar, *J. Geophys. Res., 97,* 12,187, 1992.

Wright, A. N., Dispersion and wave coupling in inhomogeneous MHD waveguides, *J. Geophys. Res., 99,* 159, 1994.

Wright, A. N., and G. J. Rickard, A numerical study of resonant absorption in a magnetohydrodynamic cavity driven by a broadband spectrum, *Ap. J., 444,* 458, 1995.

Ziesolleck, C. W. S., and D. R. McDiarmid, Auroral latitude Pc5 field line resonances: Quantized frequencies, spatial characteristics, and diurnal variation, *J. Geophys. Res., 99,* 5817, 1994.

Ziesolleck, C. W. S., and D. R. McDiarmid, Statistical survey of auroral latitude Pc5 spectral and polarization characteristics, *J. Geophys. Res.,* in press, 1995.

G. J. Rickard and A. N. Wright, Department of Mathematical and Computational Sciences, University of St. Andrews, St. Andrews, Fife KY16 9SS, Scotland. (e-mail: grahamr@dcs.st-and.ac.uk, andy@dcs.st-and.ac.uk)

(Received January 24, 1995; revised June 5, 1995; accepted June 8, 1995.)